Single-Molecule Force-Clamp Experiments Reveal Kinetics of Mechanically Activated Silyl Ester Hydrolysis

Sebastian W. Schmidt,[†,‡,§] Pavel Filippov,[†] Alfred Kersch,[†] Martin K. Beyer,[‡,*] and Hauke Clausen-Schaumann[†,§,*]

[†]Department of Precision- and Micro-Engineering, Engineering Physics, Munich University of Applied Sciences, Lothstr. 34, 80335 Munich, Germany, [‡]Institut für Physikalische Chemie, Christian-Albrechts-Universität zu Kiel, Olshausenstr. 40, 24098 Kiel, Germany, and [§]Center for NanoScience, Ludwig-Maximilians-Universität, Geschwister-Scholl-Platz 1, 80539 Munich, Germany

ABSTRACT

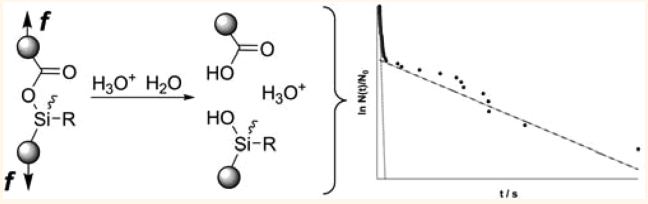

We have investigated the strength of silyl ester bonds formed between carboxymethylated amylose (CMA) molecules and silane-functionalized silicon oxide surfaces using AFM-based single-molecule force spectroscopy in the force-clamp mode. Single tethered CMA molecules were picked up, and bond lifetimes were determined at constant clamp forces of 0.8, 1.0, and 1.2 nN at seven temperatures between 295 and 320 K at pH 2.0. The results reveal biexponential rupture kinetics. To obtain the reaction rate constants for each force and temperature individually, the results were analyzed with a biexponential kinetic model using the maximum likelihood estimation (MLE) method. The force-independent kinetic and structural parameters of the underlying bond rupture mechanisms were extracted by fitting the entire data set with a parallel MLE fit procedure using the Zhurkov/Bell model and, alternatively, an Arrhenius kinetics model combined with a Morse potential as an analytic representation of the binding potential. With activation energies between 37 and 40 kJ mol^{-1}, and with Arrhenius prefactors between 5×10^4 and 2×10^6 s^{-1}, the results point to the hydrolysis of the silyl ester bond.

KEYWORDS: single-molecule force spectroscopy · force-clamp spectroscopy · silyl ester · acyloxysilane · hydrolysis · mechanochemistry

Mechanical experiments with single molecules provide direct access to the forces involved in protein folding,[1] intramolecular reorganization,[2,3] receptor–ligand interaction,[4–7] or chemical binding.[8–14] Because mechanical and thermal activation act in concert, the observed bond strength typically depends on the rate at which the mechanical load is applied. In dynamic single-molecule force spectroscopy, individual molecules are stretched at constant pulling velocities. In order to extract kinetic and structural parameters of the underlying bond rupture mechanism, the pulling velocity has to be varied over several orders of magnitude and force-loading rate-dependent bond rupture forces have to be determined. The kinetic and structural parameters can then be extracted from the offset, slope, and scattering of the rupture force *versus* force-loading rate data.[13] However, if more than one reaction pathway is present at a time, the scattering of the data increases, and as a result, the same data set can be fitted with different parameter sets, rendering the extraction of the kinetic and structural parameters virtually impossible. In single-molecule force-clamp experiments, on the other hand, bond survival times are directly measured at constant clamp forces and defined temperatures.[10,15–20] Here, different subsets of reactive sites can be clearly distinguished, and the corresponding bond lifetimes can be directly determined from the different slopes when the number of intact bonds is plotted *versus* time in a semilogarithmic representation. An Arrhenius plot then immediately renders the force-dependent activation energies and Arrhenius prefactors, and finally, these force-dependent parameters can be directly converted into force-independent kinetic and structural parameters, that is, activation energies and Arrhenius prefactors at zero force, as well as the widths of the binding potentials, by using an Arrhenius kinetic model with a force-dependent activation barrier.

* Address correspondence to clausen-schaumann@hm.edu, beyer@phc.uni-kiel.de.

Received for review October 25, 2011 and accepted January 17, 2012.

Published online January 17, 2012
10.1021/nn204111w

In a recent study,[21] we have shown that under acidic conditions (pH 2.0) single carboxymethylated amylose (CMA) polymers can be covalently tethered to a silane-coated glass substrate and a silanized AFM tip *via* a proton-catalyzed ester condensation between the carboxyl groups of CMA and free hydroxyl groups at the glass surface as well as free silanol groups of the silane. Because their hydrolytic lability strongly depends on the side-chain functionalities attached to the silicon atom,[22−24] silyl esters represent a promising intermediate for the preparation of degradable polymeric materials.[25−30] Taking advantage of their tunable stabilities, silyl ester linkages are ideally suited to improve the controlled material degradation in a variety of applications, such as carriers for drug delivery systems, matrices in tissue engineering, and temporary prosthetic devices, but also in agriculture and packaging technology.[31−34] In contrast to the desired degradation after a defined lifespan, in a number of potential applications, for example, tissue engineering or prosthetic devices, even degradable materials have to withstand considerable mechanical forces. Mechanical tension can, however, significantly accelerate the degradation process by tilting the potential energy landscape and lowering activation barriers, possibly leading to premature material fatigue or failure. In order to provide a better understanding of the role of mechanical activation in the hydrolysis mechanism, in the present study, we have made use of the possibility to covalently link CMA polymers to silane-functionalized silicon oxide surfaces *via* proton-catalyzed silyl ester condensation to investigate the hydrolysis of the silyl ester under mechanical load, using AFM-based single-molecule force spectroscopy in the force-clamp mode.

Interestingly, for all three clamp forces and all seven temperatures that we have investigated, we observed biexponential bond rupture kinetics, indicating that the ensemble of molecules is composed of two different subsets which exhibit significantly different rate constants for bond scission. Fitting the entire data set in parallel with two different Arrhenius kinetic models using maximum likelihood estimation (MLE)[35] yields the force and temperature-independent parameters of both bond rupture channels.

Apart from probing the underlying chemistry of mechanically activated silyl ester hydrolysis, this study also highlights the potential advantages (and disadvantages) of single-molecule force spectroscopy in the force-clamp mode compared to the more frequently used dynamic force spectroscopy: So far, experiments in the force-clamp mode have been limited to forces below 500 pN[10,15−20] since the probed molecules were not anchored covalently. However, for the mechanical activation of most covalent chemical bonds, nanonewton forces are required. Covalent anchoring of polymers, as used in the present study, allows applying clamp forces in the nanonewton regime, thereby extending the capabilities of the force-clamp method to the realm of covalent mechanochemistry. Furthermore, unlike the more commonly used least-squares fit, the MLE method used for data analysis accurately accounts for the exponential (non-Gaussian) probability distribution of the force-clamp data and provides statistically well-defined (asymmetric) errors. A parallel fit procedure using MLE further improves the accuracy of the fit.

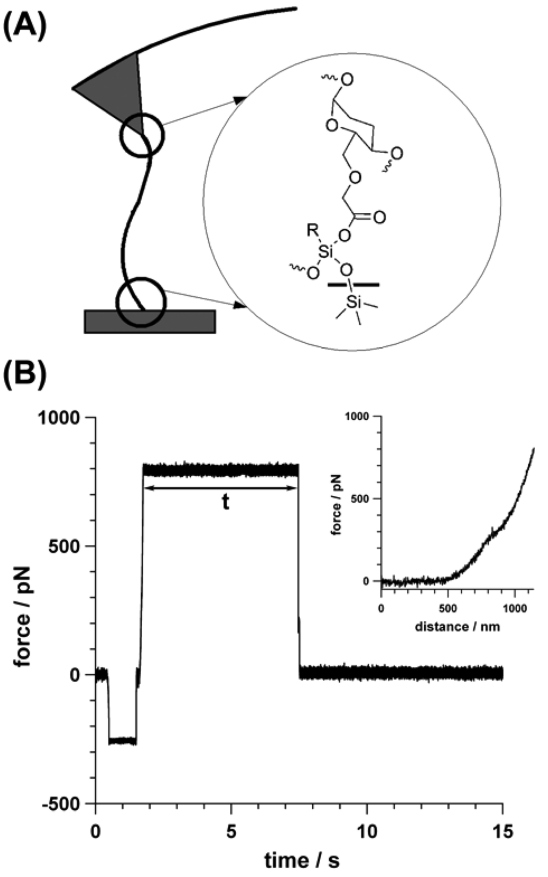

Figure 1. (A) Coupling of an individual CMA molecule between the AFM tip and a silanized glass substrate *via* acid-catalyzed ester condensation between carboxylic acids in the CMA and unreacted silanol groups in the surface anchor. (B) Typical force-clamp experiment of an individual CMA molecule covalently tethered between the substrate and the AFM tip at 295 K. Initially, the AFM tip approaches the substrate and is pressed to the substrate at a force of 250 pN for 1 s. In a few percent of all approaches, an individual CMA molecule is then randomly picked up and stretched until the clamp force of 0.8 nN is reached (cf. Methods section for a detailed description). The clamp force is kept constant until the bond ruptures after 5.69 s in this individual example. Inset: the corresponding force−distance curve shows a pronounced plateau at around 0.3 nN. Further extension leads to a sharp force increase until the clamp force is reached.

RESULTS AND DISCUSSION

A typical AFM-based force-clamp experiment, where CMA was coupled between an AFM tip and the substrate *via* acid-catalyzed ester condensation at pH 2.0 and 295 K, is displayed in Figure 1. An individual CMA

molecule is picked up and stretched until the clamp force of 0.8 nN is reached. After a clamp time $t = 5.69$ s, the bond ruptures and the force drops to zero. The corresponding force−distance curve (Figure 1B, inset) exhibits a plateau at around 0.3 nN. This nonlinear behavior has been shown to be characteristic for CMA in previous studies and allows verifying that the binding event of a single CMA polymer was detected.[8,36−39] Note that because the silyl ester bonds form efficiently only at pH 2.0 with the protocol used,[21] all experiments were conducted under these acidic conditions.

The results of 63 single-molecule force-clamp experiments at 0.8 nN clamp force and 295 K are displayed in Figure 2, where the relative number of surviving bonds $N(t)/N_0$ ($N_0 = 63$) is plotted *versus* time in a semilogarithmic representation (black dots). As can be seen from the data, the bond decay follows a biexponential kinetics, with a slow and a fast decay channel.

In order to extract the temperature and force-dependent rate constants k_1 and k_2 of the bond rupture, the data set was analyzed by fitting a normalized biexponential probability distribution of the form

$$\rho(t, a, k_1, k_2) = ak_1e^{-k_1t} + (1 - a)k_2e^{-k_2t} \quad (1)$$

to the data, using MLE combined with an evolutionary optimization algorithm. Here $\rho(t,a,k_1,k_2)dt$ represents the probability that a bond rupture is observed between time t and $t + dt$; k_1 and k_2 are the reaction rate constants at a certain temperature and clamp force; a and $(1 - a)$ correspond to the relative contributions of channels 1 and 2, respectively. To correctly account for the device-dependent lower detection limit, that is, undetectable clamp times below $t_{min} = 0.005$ s, eq 1 was renormalized to

$$\rho_{RN}(t, a, k_1, k_2) = \frac{1}{\omega}[ak_1e^{-k_1t} + (1 - a)k_2e^{-k_2t}] \quad (2)$$

where $\omega = ae^{-k_1t_{min}} + (1 - a)e^{-k_2t_{min}}$ (cf. Supporting Information for details of the fitting procedure).

For the data shown in Figure 2, the fit yields rate constants of $k_1 = 0.09\ s^{-1}$ for the slow channel and $k_2 = 6.29\ s^{-1}$ for the fast channel, as well as a fraction of 21% ($a = 0.21$) of the bonds decaying *via* the slow and 79% *via* the fast process.

Integration of eq 1 again gives the relative number of surviving bonds depicted in Figure 2:

$$\frac{N(t)}{N_0} = 1 - \int_0^t \rho(t', a, k_1, k_2)dt'$$
$$= ae^{-k_1t} + (1 - a)e^{-k_2t} \quad (3)$$

Using the values k_1, k_2, and a determined by the fit, the relative number of surviving bonds $N(t)/N_0 = ae^{-k_1t} + (1 - a)e^{-k_2t}$ (solid line) as well as the corresponding single exponential decays ae^{-k_1t} (dashed line) and $(1 - a)e^{-k_2t}$ (dotted line) were calculated and are displayed in Figure 2 together with the experimental data.

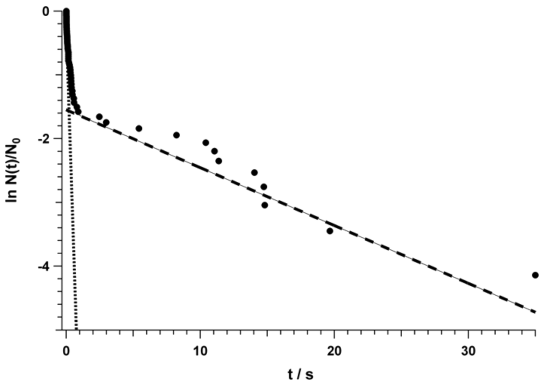

Figure 2. Bond lifetimes extracted from 63 single-molecule force-clamp experiments, where CMA was stretched between the AFM tip and the substrate under acidic conditions ($f = 0.8$ nN, $T = 295$ K). The natural logarithm of the relative fraction of intact bonds ($\ln N(t)/N_0$, *y*-axis) is plotted against the time (t, *x*-axis). The observed decay obeys a biexponential rate law (thin straight line) consisting of a slow process with $k_1 = 0.09\ s^{-1}$ (dashed line) and a fast process with $k_2 = 6.29\ s^{-1}$ (dotted line), contributing 21 and 79%, respectively, to the overall process.

It should be pointed out that the MLE method requires properly normalized probability distributions. Using the renormalized biexponential probability distribution $\rho_{RN}(t,a,k_1,k_2)$ rather than the relative number of surviving bonds $N(t)/N_0$ for the fitting procedure therefore allows for using the MLE method. Unlike a least-squares fit to $N(t)/N_0$, the MLE method correctly accounts for the non-normal probability distribution, as well as the device-dependent detection limit of 0.005 s. Directly fitting the data with eq 3, using a least-squares fit algorithm, yields comparable results (cf. Supporting Information). Nevertheless, in this case, both the exponential instead of normal nature of the underlying probability distribution as well as the detection limit of the instrument are not correctly accounted for.[35,40]

The results of the experiment depicted in Figure 2 as well as the results of similar experiments carried out at different temperatures and different clamp forces are illustrated in Figure 3, where the natural logarithm of the temperature and force-dependent rate constants k_1 (triangles) and k_2 (circles) is plotted *versus* $1000/T$ for 0.8 nN (open symbols) and 1.0 nN clamp force (black symbols) in an Arrhenius plot (cf. Supporting Information). As expected for a thermally and mechanically activated process, a trend toward increasing rate constants with increasing clamp forces as well as increasing temperatures can be observed both for k_1 and k_2.

Fitting an Arrhenius equation $k_i = A_i\exp[-E_{a,i}/(k_BT)]$ ($i = 1, 2$) to the data visualized in Figure 3 would, in principle, allow for determining activation energies and Arrhenius prefactors for the two decay channels at clamp forces of 0.8 and of 1.0 nN, respectively. However, due to the external clamp force, the bond scission is greatly accelerated in these data sets. In order to extract the force-independent activation

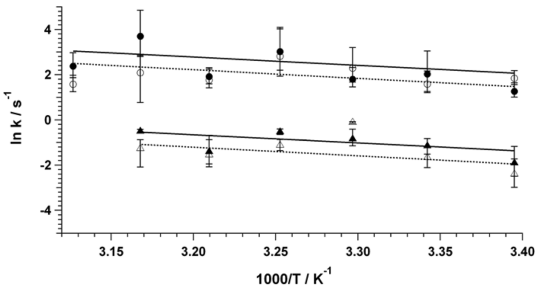

Figure 3. Arrhenius plot: logarithm of the extracted rate constants k_1 (triangles) and k_2 (circles) is plotted *vs* 1000/*T* for 0.8 nN (open symbols) and 1.0 nN clamp force (black symbols). The corresponding values for k_1, k_2, and *a* are also summarized in the Supporting Information. The four lines correspond to temperature-dependent rate constants at 0.8 and 1.0 nN, calculated with the parameters determined by a global fit of the Zhurkov/Bell model. From top to bottom: k_2 at 1.0 nN, k_2 at 0.8 nN, k_1 at 1.0 nN, and k_1 at 0.8 nN. The error bars correspond to the asymmetric one-standard-deviation parameter errors as calculated with MINOS (cf. Supporting Information).

energies and Arrhenius prefactors (at zero force), one has to account for the fact that the activation energy is usually lowered by the external force. We have therefore included force-dependent activation energies $E_{a,i}(f)$ into the Arrhenius equation. To estimate the functional relationship between the activation energy and the applied force, we have used two different models.

As a first approximation, we have used the well-established model introduced by Zhurkov and Bell,[41,42] where the height of the activation barrier depends linearly on the applied force: The force lowers activation barriers by $f\Delta x_i^{\ddagger}$ and, in turn, decreases the bond lifetimes τ_i, that is, increases the reaction rate constants $k_i = 1/\tau_i$. Here *f* denotes the applied force and $\Delta x_i^{\ddagger}$ the projection of the distance between potential minimum and transition state on the pulling direction. In the Zhurkov/Bell model, however, the $\Delta x_i^{\ddagger}$ values are assumed to be force-independent parameters, a simplification which is usually justified at small forces. However, at forces in the nanonewton regime used here, this approximation may fail.

As a second, more sophisticated, approach, which more accurately accounts for the high forces needed for the activation of covalent bonds, we have therefore used a Morse potential $V_i(x) = D_{e,i}(1 - \exp(-\beta_i x))^2$ as a one-dimensional representation of the binding potential and superimposed a constant force field[43−46] $V_{eff,i}(x,f) = V_i(x) - fx$. In this case, the force-dependent activation energies become[44,45]

$$E_{a,i}(f) = D_{e,i}\left\{\sqrt{1-\frac{f}{f_{max,i}}} - \frac{f}{f_{max,i}}\tanh^{-1}\left(\sqrt{1-\frac{f}{f_{max,i}}}\right)\right\} - \frac{\alpha}{2}h\nu_i \quad (4)$$

with $f_{max,i} = V'_{max,i} = 1/2D_{e,i}\beta_i$, the dissociation energies $D_{e,i}$, the widths of the Morse potentials β_i^{-1}, and $\alpha/2 \cdot h\nu_i$ accounting for the contribution of the zero-point energy (cf. also ref 13). First quantum chemical (DFT) calculations indicate that the contributions from the ground state and the transition state to the zero-point energy almost cancel each other. We have therefore set α equal to zero. In this case, $E_{a,i}$ at zero force and $D_{e,i}$ are equal. Unlike the linear Zhurkov/Bell model, the Morse potential-based model accounts for the fact that for the activation of covalent bonds at high forces, $\Delta x_i^{\ddagger}$ decreases with increasing force, becoming zero at $f = f_{max}$.[44−46]

Inserting the Arrhenius equation with the force-dependent activation energies $E_{a,i}(f)$ into the renormalized rate equation (eq 2) yields normalized bond rupture probability distributions $\rho_{RN}(t,T,f)$, which are functions of time, temperature, and force. These distributions allow for analyzing the entire data (bond survival times determined at all 7 temperatures and 3 clamp forces) in a parallel fit procedure using the MLE method. The free parameters are the Arrhenius prefactors A_i, activation energies $E_{a,i}$, the relative contribution of channel 1 to the overall bond rupture process *a*, and potential widths ($\Delta x_i^{\ddagger}$ in the case of the Zhurkov/Bell model and β_i^{-1} in the case of a Morse potential). Unlike k_1 and k_2, these parameters are temperature- and force-independent.

The free parameters determined by the parallel fit procedure are summarized in Table 1, both for the Zhurkov/Bell model and for the Morse potential-based model. With 37 and 38 kJ mol^{-1} in the Zhurkov/Bell model as well as 39 and 40 kJ mol^{-1} for the Morse potential-based model, the activation energies are almost identical for the two decay channels. They vary only by 2 kJ mol^{-1} with the model used, less than the error limits of ±5−7 kJ mol^{-1}; that is, both models yield essentially the same result. These values are within the typical range of activation energies for silyl ester hydrolysis, which lie between 36 and 43 kJ mol^{-1}.[47,48] Furthermore, the fact that both models yield essentially identical results also indicates that, at clamp forces around 1 nN, the linear approximation made by the Zhurkov/Bell model is still valid for this particular bond rupture mechanism.

The Arrhenius prefactors for the two decay channels are 5.5 × 10^4 s^{-1} (Zhurkov/Bell) and 5.9 × 10^4 s^{-1} (Morse) for the slow process as well as 1.9 × 10^6 s^{-1} (Zhurkov/Bell) and 2.0 × 10^6 s^{-1} (Morse) for the fast process, which is again in good agreement with Arrhenius prefactors reported for silyl ester hydrolysis[47] and which is several orders of magnitude smaller than attempt frequencies predicted for homolytic rupture processes.[44,45,49] Using the Arrhenius equation to calculate the force-independent reaction rate constants $k_1(f = 0)$ and $k_2(f = 0)$ at room temperature (295 K) yields values of 1.5 × 10^{-2} and 3.5 × 10^{-1} s^{-1} for the Zhurkov/Bell model as well as 7.3 × 10^{-3} and 1.6 × 10^{-1} s^{-1} for the Morse potential-based model, both pointing to the typically rapid hydrolysis of silyl esters.[27,47,50,51]

For better comparison of the two models, for the Morse potential-based model, Table 1 lists not only the

TABLE 1. Model-Dependent Parameters

		experimental data[a]	
model	parameter	process 1	process 2
Zhurkov/Bell	E_a/kJ mol^{-1}	$37\ ^{+7}_{-7}$	$38\ ^{+6}_{-6}$
	A/s^{-1}	$5.5 \times 10^4\ ^{+1.4 \times 10^4}_{-1.5 \times 10^4}$	$1.9 \times 10^6\ ^{+3.0 \times 10^5}_{-3.0 \times 10^5}$
	$\Delta x^{\ddagger}$/Å	$0.120\ ^{+0.034}_{-0.034}$	$0.123\ ^{+0.027}_{-0.027}$
Morse[b]	D_e/kJ mol^{-1}	$39\ ^{+6}_{-6}$	$40\ ^{+5}_{-5}$
	A/s^{-1}	$6.0 \times 10^4\ ^{+1.9 \times 10^4}_{-1.9 \times 10^4}$	$2.0 \times 10^6\ ^{+5.2 \times 10^5}_{-5.3 \times 10^5}$
	β^{-1}/Å	$0.032\ ^{+0.035}_{-0.016}$	$0.033\ ^{+0.020}_{-0.012}$
	$\Delta x^{\ddagger}$ (0.8 nN)[c]/Å	$0.125\ ^{+0.093}_{-0.054}$	$0.126\ ^{+0.065}_{-0.044}$
	$\Delta x^{\ddagger}$ (1.0 nN)[c]/Å	$0.117\ ^{+0.084}_{-0.050}$	$0.119\ ^{+0.053}_{-0.048}$

[a] According to the biexponential fit, the overall decay process is subdivided into two fractions, where process 1 contributes 28% and process 2 72% to the overall decay process. Asymmetric one-standard-deviation parameter errors were calculated with MINOS (cf. Supporting Information). [b] Here $E_a = D_e$ because $\alpha = 0$.[13]. [c] Corresponds to the force-dependent distance between reactant state and transition state in the Morse potential under mechanical load.

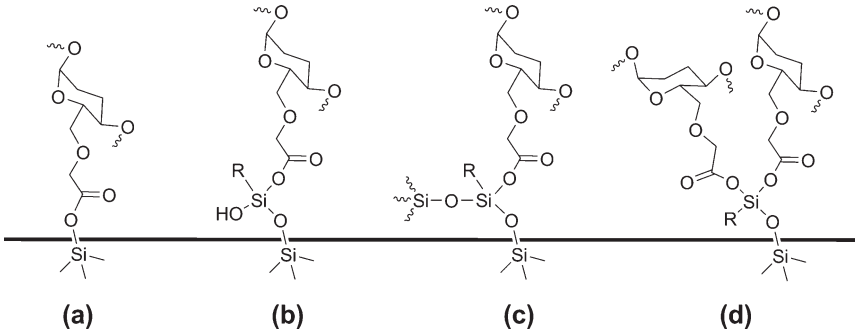

Scheme 1. Carboxymethylated amylose tethered to the surface *via* free silanol groups.

fit-parameters β_i^{-1} but also the distances $\Delta x_i^{\ddagger}$ between transition states and potential minima at 0.8 and 1.0 nN. (As mentioned above, in the Morse potential-based model, $\Delta x_i^{\ddagger}$ values are force-dependent.) Again, for both decay channels and both models, the values for $\Delta x_i^{\ddagger}$ are quite close together. With values around 0.12 Å, the potential widths are rather small for chemical binding potentials. However, it has been shown in previous studies[52−54] that in mechanically activated chemical reactions, the reaction coordinate does not necessarily coincide with the pulling direction. In this case, the observed potential width corresponds to the projection of the potential width on the pulling direction.

As pointed out above, the observed activation energies, Arrhenius prefactors and reaction rate constants lie well within the range expected for silyl ester hydrolysis.[47,48] At the same time, they are all significantly smaller than the values expected for homolytic bond scission.[8,44] Of all chemical bonds in the molecular chain connecting substrate surface and AFM cantilever, at pH 2.0, the silyl ester formed between carboxylic acid of CMA and a free silanol group on the silicon oxide surface or the silane surface linkers is most liable to hydrolysis.[21,47,55−57] Therefore, silyl ester hydrolysis is, in fact, the most plausible explanation for the observed bond rupture process.

Taking into account that the hydrolytic liability of silyl esters strongly depends on the side-chain functionalities of the silicon atom,[22−28] a reasonable explanation for the presence of two distinguishable subsets of molecules could be the presence of different chemical moieties at the silicon atom in the silyl ester linkage. As shown in Scheme 1, a silyl ester can be formed between carboxylic acids of CMA and two different chemical moieties on the substrate as well as AFM cantilever surface, that is, free hydroxyl groups on silicon oxide (Scheme 1a) and free silanol groups of surface-linked organosilanes (Scheme 1b,c).[21] Another possible side-chain difference could arise from the fact that the organosilanes used in the experiments contain three silanol groups. Only one of these silanol groups is

needed to form the silyl ester linkage with the carboxylic acid of CMA. As shown in Scheme 1b–d, of the remaining two silanol groups, either one or two groups can be connected to hydroxyl groups on the surface or to neighboring organosilanes or to an additional CMA.[58] Whether these alternative surface anchors are indeed responsible for the observation of the biexponential behavior and, if so, which configurations correspond to the two decay channels observed in the experiments remains open and has to be clarified by enhanced quantum chemical simulations, for example, with an explicitly included external force field (EFEI).[59,60]

CONCLUSION

AFM-based single-molecule force-clamp experiments clearly show that, under acidic conditions, the decay of silyl ester bonds which have been formed *via* acid-catalyzed condensation between carboxylic acids of CMA molecules and silanized substrates follows a biexponential kinetics. The force and temperature-independent kinetic and structural parameters of the underlying bond rupture process were extracted using two alternative Arrhenius kinetic models, one with a linear force dependence of the activation barrier and another one where a Morse potential has been used as a one-dimensional representation of the binding potential. The observed kinetic parameters *i.e.*, activation barriers, Arrhenius prefactors, and reaction rate constants all agree well with silyl ester hydrolysis.

To clarify which side groups of the silicon atom account for the biexponential behavior, combined quantum chemical and molecular dynamics simulations have to be carried out. Nevertheless, our results already provide a better understanding of the mechanochemical degradation of silyl-ester-containing materials: With the force-dependent Arrhenius equation and the fit parameters listed in Table 1, reaction rate constants can be derived as a function of force and temperature, which is particularly valuable when it comes to the stress resistance and mechanical toughness of silyl-ester-containing polymeric materials as well as for the design of new smart materials, such as force sensing materials or materials with defined lifetimes under mechanical load.

Compared to dynamic force spectroscopy, which is performed at constant pulling velocities, single-molecule force-clamp experiments yield data with a higher content of information. Multiexponential decay kinetics become clearly evident in the force-clamp data, while in dynamic experiments, they lead to a rather unspecific broadening of the rupture force distribution. Since the data reveal more details of the underlying reactions, superior modeling becomes possible. When the MLE method is applied, force-clamp data can be modeled with proper assumptions for the bond rupture probability distributions. Meaningful, statistically precisely defined error limits can be derived within the MLE model. Using a parallel, rather than a stepwise fit procedure greatly increases the size of the statistical ensemble and thus further improves the accuracy of the fit. The results presented here suggest that the combination of force-clamp experiments with the maximum likelihood estimation provides a powerful method for the quantitative investigation of covalent mechanochemistry.

METHODS

Materials. N^1-[3-(Trimethoxysilyl)propyl]diethylenetriamine (DETA), carboxymethylated amylose (CMA), and phosphate buffered saline (PBS; buffer composed of 0.137 M NaCl, 0.010 M Na_2HPO_4, 0.003 M KCl, and 0.002 M KH_2PO_4, pH 7.4 at T = 298 K) were purchased from Sigma-Aldrich (Deisenhofen, Germany). Hydrochloric acid (32% GR for analysis), acetic acid (99–100% for synthesis), and ethanol (absolute GR for analysis) were obtained from Merck (Darmstadt, Germany). All experiments were conducted with silicon nitride AFM cantilevers with a nominal force constant between 10 and 20 mN/m (MLCT-AU, Veeco Instruments GmbH, Mannheim, Germany). Glass microscope slides from Menzel (Braunschweig, Germany) were used as substrates.

Sample Preparation. Silanization of glass microscope slides and AFM tips was performed according to a previously presented method.[21] In brief, glass substrates were cleaned in diluted hydrochloric acid in double distilled water (H_2O_{ddest}), sonicated in this solution, and rinsed three times with H_2O_{ddest}. To remove organic contaminations from the AFM tip, cantilevers were irradiated with UV light and immersed in ethanol. AFM tip and glass surfaces were functionalized using a solution of ethanol and H_2O_{ddest}, which was acidified with diluted acetic acid to pH 4.5–5.5. Afterward, DETA was added, and both slides and cantilevers were incubated in this solution, rinsed with ethanol, and cured at 110 °C. Silanized glass slides and AFM tips were then stored in vacuum at room temperature. Prior to individual force spectroscopy experiments, 10 mg of CMA was suspended in 1 mL of PBS, which was titrated to pH 2.0 with diluted hydrochloric acid. This solution was transferred to the DETA-functionalized microscope slide, and after a reaction period of 10 min, the slide was thoroughly rinsed with acidic PBS buffer in order to remove noncovalently bound CMA from the substrate.

Single-Molecule Force Spectroscopy. The optical lever sensitivity and cantilever force constant were determined based on the thermal noise method prior to every individual force-clamp experiment,[61] and the average value of three independent measurements was used. Then, the prepared slide was mounted on the AFM stage and covered with several hundred microliters of PBS buffer at pH 2.0. The temperature of the solution was controlled by a custom-built resistance heating stage and measured with a Pt100/1 temperature sensor (Bürklin OHG, Oberhaching, Germany). Prior to AFM measurements, the temperature of the solution on the stage was adjusted and, after equilibrium was obtained, kept constant during experiments. Then, the functionalized AFM tip bearing multiple binding sites (*i.e.*, free hydroxyl groups) was repetitively brought into contact with individual carboxyl groups from the CMA molecules, which were covalently tethered to the glass substrate. In the case of a successful bond formation, the tethered molecule was stretched with the predefined clamp force until a bond rupture event occurred. Then the next cycle was started and the substrate surface was again approached by the AFM cantilever.

In order to increase the number of detected binding events, a grid of at least 64 contact spots within a surface area of 10 μm^2 was repeatedly approached and CMA was randomly picked up from the surface. All force-clamp experiments were conducted with a NanoWizard atomic force microscope (JPK Instruments, Berlin, Germany) in the force spectroscopy mode. In the implemented Force RampDesigner, the clamp retract speed (*i.e.*, the z-piezo retraction velocity) was adjusted to 5 $\mu m\ s^{-1}$ and the clamp P and I gains were tuned for every AFM tip individually according to the approach gains. In all cases, the contact force between the AFM tip and the substrate prior to conducting a force-clamp experiment was kept below 0.3 nN, and the contact time between the AFM tip and the substrate was set to 1.0 s. In control experiments at neutral pH, no binding events were detected under these experimental conditions.[21] In order to ensure that one individual CMA molecule is investigated at a time, every force *versus* time curve was converted to a force–distance curve and analyzed with regard to the characteristic plateau at around 0.3 nN. On the basis of the individual gain settings adapted for the cantilevers used (*i.e.*, gains depending on the cantilever resonance frequency), the minimum detection time turned out to be 0.005 s in our experiments. Depending on the experimental conditions, a peak-to-peak force noise between 10 and 50 pN was observed, and the force resolution was always <10 pN.

Conflict of Interest: The authors declare no competing financial interest.

Acknowledgment. The authors would like to thank M. Pill for providing DFT simulations and helpful discussions. S.W.S. and H. C.-S. gratefully acknowledge financial support of the German Excellence Initiative *via* the "Nanosystems Initiative Munich (NIM)". M.K.B. gratefully acknowledges startup funds from the Sonderforschungsbereich 677 "Function by Switching" supported by the Deutsche Forschungsgemeinschaft.

Supporting Information Available: Details of data analysis and calculation of parameter errors. This material is available free of charge *via* the Internet at http://pubs.acs.org.

REFERENCES AND NOTES

1. Rief, M.; Gautel, M.; Oesterhelt, F.; Fernandez, J. M.; Gaub, H. E. Reversible Unfolding of Individual Titin Immunoglobulin Domains by AFM. *Science* **1997**, *276*, 1109–1112.
2. Smith, S. B.; Finzi, L.; Bustamante, C. Direct Mechanical Measurements of the Elasticity of Single DNA Molecules by Using Magnetic Beads. *Science* **1992**, *258*, 1122–1126.
3. Rief, M.; Clausen-Schaumann, H.; Gaub, H. E. Sequence-Dependent Mechanics of Single DNA Molecules. *Nat. Struct. Biol.* **1999**, *6*, 346–349.
4. Florin, E. L.; Moy, V. T.; Gaub, H. E. Adhesion Forces between Individual Ligand–Receptor Pairs. *Science* **1994**, *264*, 415–417.
5. Hinterdorfer, P.; Baumgartner, W.; Gruber, H. J.; Schilcher, K.; Schindler, H. Detection and Localization of Individual Antibody–Antigen Recognition Events by Atomic Force Microscopy. *Proc. Natl. Acad. Sci. U.S.A.* **1996**, *93*, 3477–3481.
6. Merkel, R.; Nassoy, P.; Leung, A.; Ritchie, K.; Evans, E. Energy Landscapes of Receptor–Ligand Bonds Explored with Dynamic Force Spectroscopy. *Nature* **1999**, *397*, 50–53.
7. Schwesinger, F.; Ros, R.; Strunz, T.; Anselmetti, D.; Guntherodt, H. J.; Honegger, A.; Jermutus, L.; Tiefenauer, L.; Pluckthun, A. Unbinding Forces of Single Antibody–Antigen Complexes Correlate with Their Thermal Dissociation Rates. *Proc. Natl. Acad. Sci. U.S.A.* **2000**, *97*, 9972–9977.
8. Grandbois, M.; Beyer, M.; Rief, M.; Clausen-Schaumann, H.; Gaub, H. E. How Strong is a Covalent Bond? *Science* **1999**, *283*, 1727–1730.
9. Lantz, M. A.; Hug, H. J.; Hoffmann, R.; van Schendel, P. J. A.; Kappenberger, P.; Martin, S.; Baratoff, A.; Guntherodt, H. J. Quantitative Measurement of Short-Range Chemical Bonding Forces. *Science* **2001**, *291*, 2580–2583.
10. Wiita, A. P.; Ainavarapu, S. R. K.; Huang, H. H.; Fernandez, J. M. Force-Dependent Chemical Kinetics of Disulfide Bond Reduction Observed with Single-Molecule Techniques. *Proc. Natl. Acad. Sci. U.S.A.* **2006**, *103*, 7222–7227.
11. Schwaderer, P.; Funk, E.; Achenbach, F.; Weis, J.; Bräuchle, C.; Michaelis, J. Single-Molecule Measurement of the Strength of a Siloxane Bond. *Langmuir* **2007**, *24*, 1343–1349.
12. Schmidt, S. W.; Beyer, M. K.; Clausen-Schaumann, H. Dynamic Strength of the Silicon–Carbon Bond Observed over Three Decades of Force-Loading Rates. *J. Am. Chem. Soc.* **2008**, *130*, 3664–3668.
13. Schmidt, S. W.; Kersch, A.; Beyer, M. K.; Clausen-Schaumann, H. Mechanically Activated Rupture of Single Covalent Bonds: Evidence of Force Induced Bond Hydrolysis. *Phys. Chem. Chem. Phys.* **2011**, *13*, 5994–5999.
14. Zheng, P.; Li, H. Highly Covalent Ferric-Thiolate Bonds Exhibit Surprisingly Low Mechanical Stability. *J. Am. Chem. Soc.* **2011**, *133*, 6791–6798.
15. Oberhauser, A. F.; Hansma, P. K.; Carrion-Vazquez, M.; Fernandez, J. M. Stepwise Unfolding of Titin under Force-Clamp Atomic Force Microscopy. *Proc. Natl. Acad. Sci. U.S.A.* **2001**, *98*, 468–472.
16. Fernandez, J. M.; Li, H. Force-Clamp Spectroscopy Monitors the Folding Trajectory of a Single Protein. *Science* **2004**, *303*, 1674–1678.
17. Bullard, B.; Garcia, T.; Benes, V.; Leake, M. C.; Linke, W. A.; Oberhauser, A. F. The Molecular Elasticity of the Insect Flight Muscle Proteins Projectin and Kettin. *Proc. Natl. Acad. Sci. U.S.A.* **2006**, *103*, 4451–4456.
18. Ainavarapu, S. R. K.; Wiita, A. P.; Dougan, L.; Uggerud, E.; Fernandez, J. M. Single-Molecule Force Spectroscopy Measurements of Bond Elongation during a Bimolecular Reaction. *J. Am. Chem. Soc.* **2008**, *130*, 6479–6487.
19. Szoszkiewicz, R.; Ainavarapu, S. R. K.; Wiita, A. P.; Perez-Jimenez, R.; Sanchez-Ruiz, J. M.; Fernandez, J. M. Dwell Time Analysis of a Single-Molecule Mechanochemical Reaction. *Langmuir* **2008**, *24*, 1356–1364.
20. Liang, J.; Fernandez, J. M. Kinetic Measurements on Single-Molecule Disulfide Bond Cleavage. *J. Am. Chem. Soc.* **2011**, *133*, 3528–3534.
21. Schmidt, S. W.; Christ, T.; Glockner, C.; Beyer, M. K.; Clausen-Schaumann, H. Simple Coupling Chemistry Linking Carboxyl-Containing Organic Molecules to Silicon Oxide Surfaces under Acidic Conditions. *Langmuir* **2010**, *26*, 15333–15338.
22. Hudrlik, P. F.; Feasley, R. The Reactions of Nucleophiles with Acyloxysilanes. *Tetrahedron Lett.* **1972**, *13*, 1781–1784.
23. Cunico, R. F.; Bedell, L. The Triisopropylsilyl Group as a Hydroxyl-Protecting Function. *J. Org. Chem.* **1980**, *45*, 4797–4798.
24. Gitto, S. P.; Wooley, K. L. Poly(silyl ester)s: A New Family of Hydrolytically-Degradable Polymers with Attunable Stabilities. *Macromolecules* **1995**, *28*, 8887–8889.
25. Weinberg, J. M.; Gitto, S. P.; Wooley, K. L. Synthesis and Characterization of Degradable Poly(silyl ester)s. *Macromolecules* **1998**, *31*, 15–21.
26. Wang, M.; Weinberg, J. M.; Wooley, K. L. Synthesis, Characterization and Degradation of Poly(silyl ester)s. *Macromolecules* **1998**, *31*, 7606–7612.
27. Wang, M.; Weinberg, J. M.; Wooley, K. L. Geminal Poly(silyl ester)s: Highly Labile Degradable Polymers. *J. Polym. Sci., Part A: Polym. Chem.* **1999**, *37*, 3606–3613.
28. Liu, Z.; Han, N.; Dong, J. Poly(silyl ester)s: A New Route of Synthesis *via* the Condensation of Di-*tert*-butyl Ester of Dicarboxylic Acid with Dichlorosilane. *J. Appl. Polym. Sci.* **2006**, *100*, 1378–1384.
29. Downing, C. M.; Missaghi, M. N.; Kung, M. C.; Kung, H. H. Design and Synthesis of Readily Degradable Acyloxysilane Dendrimers. *Tetrahedron* **2011**, *67*, 7502–7509.
30. Bressy, C.; Nguyen, M. N.; Tanguy, B.; Ngo, V. G.; Margaillan, A. Poly(trialkylsilyl methacrylate)s: A Family of Hydrolysable Polymers with Tuneable Erosion Profiles. *Polym. Degrad. Stab.* **2011**, *95*, 1260–1268.
31. Vert, M.; Li, S. M.; Spenlehauer, G.; Guerin, P. Bioresorbability and Biocompatibility of Aliphatic Polyesters. *J. Mater. Sci.: Mater. Med.* **1992**, *3*, 432–446.

32. Ikada, Y.; Tsuji, H. Biodegradable Polyesters for Medical and Ecological Applications. *Macromol. Rapid Commun.* **2000**, *21*, 117–132.
33. Mohanty, A. K.; Misra, M.; Hinrichsen, G. Biofibres, Biodegradable Polymers and Biocomposites: An Overview. *Macromol. Mater. Eng.* **2000**, *276*−*277*, 1–24.
34. Nair, L. S.; Laurencin, C. T. Biodegradable Polymers as Biomaterials. *Prog. Polym. Sci.* **2007**, *32*, 762–798.
35. Brandt, S. In *Data Analysis: Statistical and Computational Methods for Scientists and Engineers*, 3rd ed.; Springer Verlag: Berlin, 1998; pp 187−211.
36. Rief, M.; Oesterhelt, F.; Heymann, B.; Gaub, H. E. Single Molecule Force Spectroscopy on Polysaccharides by Atomic Force Microscopy. *Science* **1997**, *275*, 1295–1297.
37. Marszalek, P. E.; Oberhauser, A. F.; Pang, Y. P.; Fernandez, J. M. Polysaccharide Elasticity Governed by Chair-Boat Transitions of the Glucopyranose Ring. *Nature* **1998**, *396*, 661–664.
38. Li, H. B.; Rief, M.; Oesterhelt, F.; Gaub, H. E.; Zhang, X.; Shen, J. C. Single-Molecule Force Spectroscopy on Polysaccharides by AFM—Nanomechanical Fingerprint of α-(1,4)-Linked Polysaccharides. *Chem. Phys. Lett.* **1999**, *305*, 197–201.
39. Heymann, B.; Grubmüller, H. 'Chair-Boat' Transitions and Side Groups Affect the Stiffness of Polysaccharides. *Chem. Phys. Lett.* **1999**, *305*, 202–208.
40. Fraile, R.; Garcia-Ortega, E. Fitting an Exponential Distribution. *J. Appl. Meteorol.* **2005**, *44*, 1620–1625.
41. Zhurkov, S. N.; Korsukov, V. E. Atomic Mechanism of Fracture of Solid Polymers. *J. Polym. Sci., Part B: Polym. Phys.* **1974**, *12*, 385–398.
42. Bell, G. I. Models for Specific Adhesion of Cells to Cells. *Science* **1978**, *200*, 618–627.
43. Kauzmann, W.; Eyring, H. The Viscous Flow of Large Molecules. *J. Am. Chem. Soc.* **1940**, *62*, 3113–3125.
44. Beyer, M. K. The Mechanical Strength of a Covalent Bond Calculated by Density Functional Theory. *J. Chem. Phys.* **2000**, *112*, 7307–7312.
45. Hanke, F.; Kreuzer, H. J. Breaking Bonds in the Atomic Force Microscope: Theory and Analysis. *Phys. Rev. E* **2006**, *74*, 0319091–0319095.
46. Iozzi, M. F.; Helgaker, T.; Uggerud, E. Assessment of Theoretical Methods for the Determination of the Mechanochemical Strength of Covalent Bonds. *Mol. Phys.* **2009**, *107*, 2537–2546.
47. Konieczny, S.; Wojnowski, W. Beiträge zur Chemie der Silicium-Schwefel-Verbindungen. 52 [1]. Reaktion von Trialkoxysilanthiolen mit Carbonsäuren. Darstellung und Hydrolyse der Trialkoxyacyloxysilane. *Z. Anorg. Allg. Chem.* **1988**, *562*, 153–159.
48. Sharp, K. G. A Two-Component, Non-aqueous Route to Silica Gel. *J. Sol*−*Gel Sci. Technol.* **1994**, *2*, 35–41.
49. Lourderaj, U.; McAfee, J. L.; Hase, W. L. Potential Energy Surface and Unimolecular Dynamics of Stretched *n*-Butane. *J. Chem. Phys.* **2008**, *129*, 0947011–09470110.
50. Liu, G. B.; Zhao, H. Y.; Thiemann, T. Triphenylphosphine-Catalyzed Dehydrogenative Coupling Reaction of Carboxylic Acids with Silanes—A Convenient Method for the Preparation of Silyl Esters. *Adv. Synth. Catal.* **2007**, *349*, 807–811.
51. García, S. J.; Fischer, H. R.; White, P. A.; Mardel, J.; González-García, Y.; Mol, J. M. C.; Hughes, A. E. Self-Healing Anticorrosive Organic Coating Based on an Encapsulated Water Reactive Silyl Ester: Synthesis and Proof of Concept. *Prog. Org. Coat.* **2011**, *70*, 142–149.
52. Schlierf, M.; Rief, M. Single-Molecule Unfolding Force Distributions Reveal a Funnel-Shaped Energy Landscape. *Biophys. J.* **2006**, *90*, L33–L35.
53. Ribas-Arino, J.; Shiga, M.; Marx, D. Unravelling the Mechanism of Force-Induced Ring-Opening of Benzocyclobutenes. *Chem.—Eur. J.* **2009**, *15*, 13331–13335.
54. Li, W. J.; Gräter, F. Atomistic Evidence of How Force Dynamically Regulates Thiol/Disulfide Exchange. *J. Am. Chem. Soc.* **2010**, *132*, 16790–16795.
55. Bershtein, V. A.; Egorova, L. M.; Solov'ev, V. V. Disintegration of Polymers by a Hydrolytic Mechanism. *Mech. Compos. Mater.* **1977**, *13*, 715–721.
56. Mabey, W.; Mill, T. Critical Review of Hydrolysis of Organic Compounds in Water under Environmental Conditions. *J. Phys. Chem. Ref. Data* **1978**, *7*, 383–415.
57. Wang, H.; Harris, J. M. Surface Diffusion of Organosiloxane Ligands Covalently Bound to Silica. *J. Am. Chem. Soc.* **1994**, *116*, 5754–5761.
58. Arkles, B. Tailoring Surfaces with Silanes. *CHEMTECH* **1977**, *7*, 766–778.
59. Ribas-Arino, J.; Shiga, M.; Marx, D. Understanding Covalent Mechanochemistry. *Angew. Chem., Int. Ed.* **2009**, *48*, 4190–4193.
60. Ribas-Arino, J.; Shiga, M.; Marx, D. Mechanochemical Transduction of Externally Applied Forces to Mechanophores. *J. Am. Chem. Soc.* **2010**, *132*, 10609–10614.
61. Butt, H.-J.; Jaschke, M. Calculation of Thermal Noise in Atomic Force Microscopy. *Nanotechnology* **1995**, *6*, 1–7.